

Effects of uniaxial strain on the exciton spectra of CuCl, CuBr, and CuI

A. Blacha, S. Ves,* and M. Cardona

Max-Planck-Institut für Festkörperforschung, Heisenbergstrasse 1, D-7000 Stuttgart 80, Federal Republic of Germany

(Received 27 December 1982)

We have investigated the effects of large static uniaxial strain, up to ~ 3 GPa, on the excitons $Z_{1,2}$ and Z_3 of the cuprous halides using a gasketed diamond anvil cell. From the shifts and the stress-induced splittings of these excitons, we have obtained orbital and spin-orbit hydrostatic and shear deformation potentials. We have found that the shear deformation potential $d=d_1+2d_2$ is *positive* for CuCl and *negative* for CuBr and CuI. Our measurements also show that the deformation potential of the spin-orbit splitting, $d\Delta_0/d\ln V$, is *negative* for all three copper halides. From the pressure dependence of the intensity ratio $I_{Z_{1,2}}/I_{Z_3}$ we have been able to obtain reliable values for the electron-hole exchange energy of the edge excitons in CuCl and CuBr.

I. INTRODUCTION

The copper halides CuCl, CuBr, and CuI are the last members of the isoelectronic series A^nB^{8-n} with an average of four valence electrons per atom in the outer electronic shells. Under normal conditions they crystallize in the zinc-blende structure and are thus isomorphic with the III-V and II-VI compounds. A basic feature, however, separates the copper halides from the other members of the mentioned families. The valence bands of these I-VII compound semiconductors originate from the filled d^{10} shell of the Cu^+ ion and the s^2p^6 rare-gas valence configuration of the singly charged, negative halogen ions. In contrast to the III-V and II-VI compounds, whose valence bands also originate from s^2p^6 configurations, but with the energy of the occupied metal d levels well below the valence levels, the copper halides have the energy levels of the copper $3d$ electrons very close to those of the p levels of the halogen.^{1,2} This fact leads to a very heavy hybridization between the copper $3d$ electrons and the p -like electrons of the halogen, and thus increases drastically the number of valence electrons per unit formula from 8 to 18. A number of interesting properties,¹ such as the negative spin-orbit splitting of the uppermost valence band of CuCl,² can be attributed to the p - d admixture just mentioned.

During the past few years the diamond anvil cell has proved to be very useful for performing optical measurements under high hydrostatic pressure.³⁻⁸ Absorption and luminescence^{4,5} measurements have yielded hydrostatic deformation potentials. These techniques have been used to study the different phase transitions seen in copper halides as a func-

tion of pressure.^{6,8}

In this paper we present optical-absorption measurements under uniaxial strain performed with a diamond anvil cell. The study of the effects of uniaxial stress on the optical transitions of a material yields valuable information on the intrinsic properties of the material. The application of uniaxial stress, and the related strain, produces changes in the lattice parameters, and, most significantly, changes in the crystal symmetry. The changes in symmetry are reflected in the change of the electronic band structure⁹⁻¹¹ which can be revealed by measuring the optical properties.¹²⁻¹⁴ The anisotropic nature of the strain produces stress-induced splittings and shifts of the energy levels and changes in the oscillator strengths, which can be related to the properties of the undeformed crystal.^{9,15} From an analysis of the changes as a function of the magnitude of the applied stress, we have been able to determine the hydrostatic deformation potentials (a) and the deformation potentials (d) for [111] shear. In some cases, both the orbital (a_1, d_1) and the spin-dependent contributions (a_2, d_2) to these deformation potentials have been obtained. Moreover, a measurement of the intensities of the optical transitions versus pressure yields reliable values for the electron-hole exchange constant of the excitons under consideration.

II. EXPERIMENT

Optical transmission data were taken for cuprous halides under high uniaxial pressures produced with the following technique. We used a gasketed diamond anvil cell^{16,17} with a 4:1 methanol-ethanol mixture as the pressure transmitting fluid. The

TABLE I. Stiffness constants and bulk modulus of the cuprous halides in the zinc-blende phase (in GPa) (see Ref. 51). The bulk modulus under (Ref. 52) is somewhat higher than that used here as it includes stiffening due to anharmonicity at high pressures. For consistency, we use here the low-pressure values of the stiffness.

	C_{11}	C_{12}	C_{44}	$C_{ }$	C_{\perp}	B
CuCl	45.4	36.9	14.9	59.2	30.0	39.8 54.5 ^a
CuBr	45.8	35.1	14.4	57.9	29.0	39.0
CuI	45.1	30.7	18.4	60.10	23.3	35.5

^aSee Ref. 52.

samples, thin films of $\sim 2000\text{-\AA}$ thickness, were evaporated from a piece of single-crystal CuCl, CuBr, and CuI onto one of the diamond anvils of the high-pressure cell. It is known that the crystallites in the films are preferentially oriented with the [111] direction perpendicular to the substrate.^{2,18-20} For the absorption measurements we used either a xenon arc or a halogen lamp and a SPEX double monochromator with photon-counting electronics. The optical axis of the system was kept perpendicular to the substrate. The pressure inside the cell was determined by the standard ruby luminescence technique.^{16,17} The absorption spectra were obtained by comparing the transmission spectra of the system with and without sample. The resolution lay between 0.5 and 1 \AA .

From the results of the measurements performed at 100 K, we infer that the methanol-ethanol mixture, when becoming glassy at low temperatures, acts as a hard piston on the evaporated samples and produces a mixture of hydrostatic and shear stress. When similar experiments are performed at room temperature pure hydrostatic pressures are obtained: No trace of splittings of degenerate exciton levels due to shear stresses are seen in the absorption spectra. In spite of the broadening of the exciton lines at room temperature, some splitting or at least an increase in the linewidth should be seen if any significant fraction of uniaxial stress were present. This is not the case for the measurements at room temperature.

To quantify the shear component of the stress, we note that the elastic stiffness of diamond is very large in comparison with that of the copper halides (the bulk moduli of diamond and Cu X are $B = 490$ GPa and $B \simeq 40$ GPa, respectively). As the thin film is supported by the diamond substrate and the diamond is nearly incompressible, the lateral strain of the rather soft samples can be assumed to be zero. Therefore the only component of the strain tensor ($\vec{\epsilon}$) which is not equal to zero is $\epsilon_{\bar{z}\bar{z}}$, referring to a rectangular coordinate system with the \bar{z} axis perpendicular and the \bar{x} and \bar{y} axis parallel to the sur-

face of the diamond. $\epsilon_{\bar{z}\bar{z}}$ is proportional to the $\sigma_{\bar{z}\bar{z}}$ component of the stress tensor ($\vec{\sigma}$), which is, in this case, equal to the pressure p inside the anvil cell measured by the ruby manometer,

$$\sigma_{\bar{z}\bar{z}} = p = C_{||} \epsilon_{\bar{z}\bar{z}}. \quad (1)$$

We wish to write the stiffness constant $C_{||}$, which is referring to the \bar{z} axis, i.e., to the [111] direction of the samples, in terms of the stiffness constants C_{11} , C_{12} , and C_{44} , referring to the cubic crystal axes. To do this one has to transform the strain tensor ($\vec{\epsilon}$) and the stiffness tensor (\vec{C}) so that the \bar{z} axis becomes parallel to the [111] direction in the cubic system. A straightforward calculation yields for $C_{||}$,

$$C_{||} = \frac{1}{3}(C_{11} + 2C_{12} + 4C_{44}), \quad (2)$$

and for the components ϵ_{ij} of the strain tensor, now

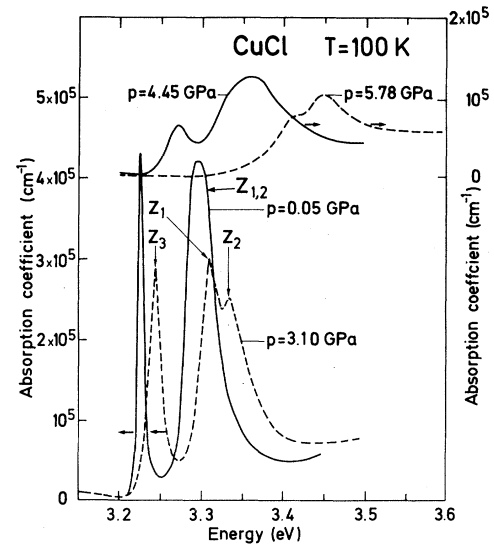


FIG. 1. Typical absorption spectra of a thin film of CuCl for various cell pressures at $T \simeq 100$ K. Data at $p = 3.1$ GPa show clearly the splitting of the exciton $Z_{1,2}$ into Z_1 and Z_2 due to the uniaxial component of the stress.

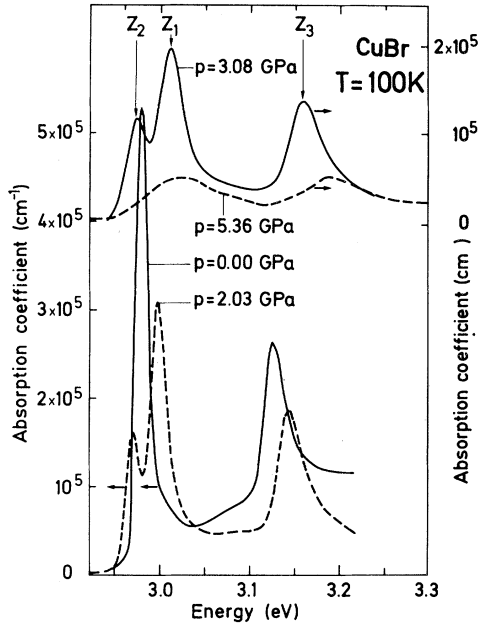


FIG. 2. Absorption spectra of a thin film of CuBr for various cell pressures p at $T \approx 100$ K. Splitting of the $Z_{1,2}$ exciton is shown clearly at $p = 2.03$ GPa.

referring to the cubic axis x, y, z ,

$$\epsilon_{ij} = \frac{\epsilon_{zz}}{3} = \frac{p}{3C_{\parallel}} \quad (3)$$

($i, j = x, y, z$). The corresponding components σ_{ij} of the stress tensor are

$$\sigma_{ii} = (C_{11} + 2C_{12})\epsilon_{zz}/3, \quad (4a)$$

$$\sigma_{ij} = 2C_{44}\epsilon_{zz}/3 \quad \text{for } i \neq j. \quad (4b)$$

Consequently, the shear components of the stress are not zero for $p > 0$. From (4a) it follows for the hydrostatical part p_H of the stress

$$p_H = \frac{1}{3} \text{trace} \vec{\sigma} = (C_{11} + 2C_{12})p / (3C_{\parallel}), \quad (5)$$

i.e., the fraction p_H/p of the measured cell pressure p acting as a hydrostatic stress is

$$p_H/p = (C_{11} + 2C_{12}) / (3C_{\parallel}) \approx 0.6 \quad (6)$$

for the copper halides (see Table I).

This is a consequence of the assumption that the evaporated samples are strained only in the direction perpendicular to the diamond anvil. In Sec. III we show that this assumption seems to hold as long as the cell pressure p is lower than an upper limit $p_1 \approx 3$ GPa. For pressures p higher than p_1 , (1) and (5) are not applicable. The stress becomes more and more hydrostatic: The hydrostatic component p_H of the pressure increases faster with p than the uniaxial one for $p > p_1$.

We want to point out one important aspect of this experimental technique which is interesting for its applications. The uniaxial strain obtained on an evaporated thin film of copper halide or a similar material can be very large. At a cell pressure $p \sim 3$ GPa it is 1–2 orders of magnitude larger than the maximum uniaxial strain one can apply without damage on bulk crystals of these rather soft materials.^{21,22} This fact makes the thin-film technique interesting for measurements of small uniaxial pres-

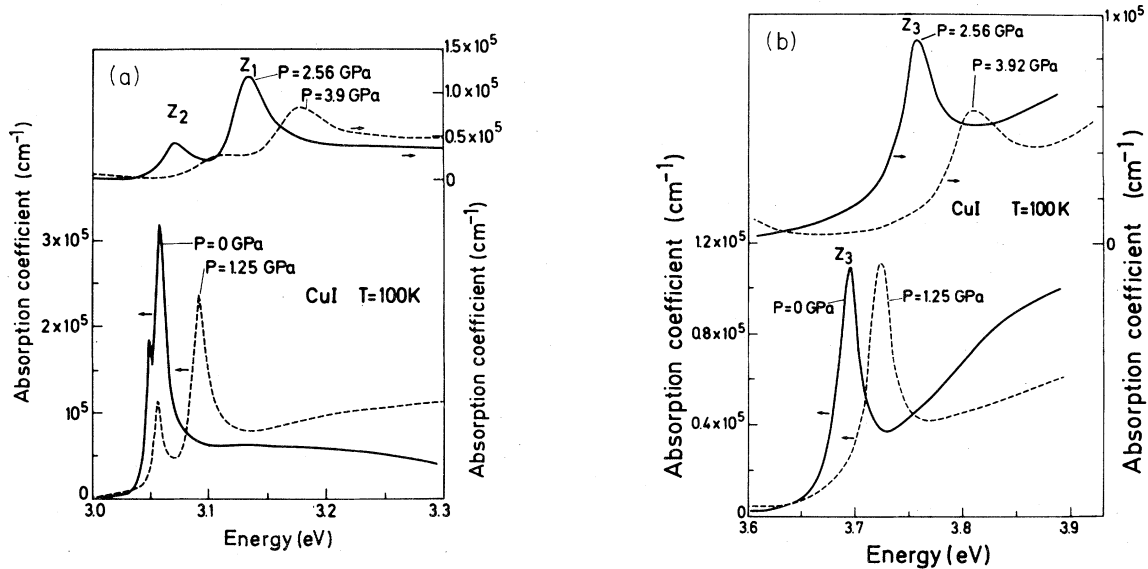


FIG. 3. (a) Absorption data of thin films of CuI at $T \approx 100$ K. Application of uniaxial stress results in the splitting of the exciton $Z_{1,2}$ into Z_1 and Z_2 . Splitting at zero pressure is due to the different thermal-expansion coefficient of substrate (diamond) and CuI. (b) Absorption spectra (Z_3) of a thin film of CuI at $T \approx 100$ K.

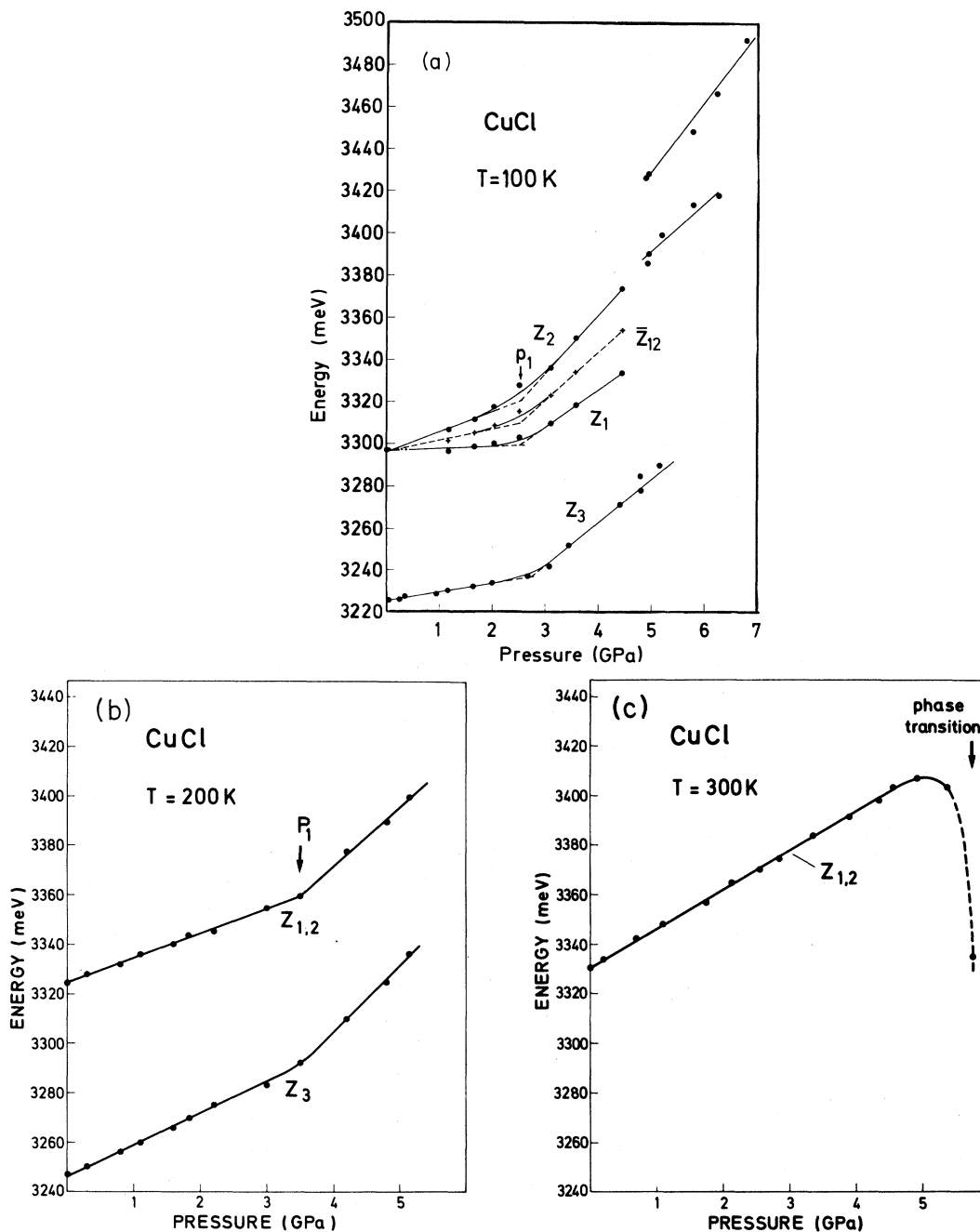


FIG. 4. (a) Pressure dependence of Z_1, Z_2, Z_3 and the average $\bar{Z}_{1,2}$ of Z_1 and Z_2 exciton peaks of CuCl at $T \approx 100$ K. p_1 indicates the point above which the pressure becomes more hydrostatic. Discontinuity of Z_2 and Z_3 at 4.8 GPa indicates a phase transition. (b) Shift of the excitons $Z_{1,2}$ and Z_3 of a thin film of CuCl at $T=200$ K. (c) Pressure dependence of the excitons peak $Z_{1,2}$ of a thin film of CuCl at $T=300$ K.

sure coefficients which can only be obtained using high pressures.

III. RESULTS

Typical absorption spectra for CuCl, CuBr, and CuI are shown in Figs. 1, 2, and 3(a) and 3(b),

respectively. At zero pressure p we see two peaks $Z_{1,2}$ and Z_3 . Peak $Z_{1,2}$ is related to the lowest excitonic excitation of electrons in the fourfold Γ_8 valence band. Peak Z_3 is related to transitions from the (twofold Γ_7) spin-orbit split-off band to the exciton ground state.^{1,2}

Upon application of pressure the peak $Z_{1,2}$ splits into Z_1 and Z_2 , a sure sign of the existence of a uniaxial stress component in the [111] direction, as explained in Sec. II. This stress component lifts the fourfold degeneracy of the Γ_8 valence-band state and causes a splitting into $\Gamma_{4,5}$ and Γ_6 components (representations of the C_{3v} space group).^{23,24}

Comparing Figs. 1 and 2 or 3 we see first that the order of the peaks $Z_{1,2}$ and Z_3 is inverted in CuCl with respect to CuBr and CuI. This is known to be due to the fact that the spin-orbit splitting $\Delta_0 = E(Z_3) - E(Z_{1,2})$ is negative in the case of CuCl and positive in the case of CuBr and CuI ($\Delta_0 = -70$ meV for CuCl and 150 or 640 meV for CuBr and CuI at zero pressure).² A second noteworthy point is the different order of the excitons Z_1 and Z_2 : In the case of CuCl the energy of Z_1 is lower than the energy of Z_2 , whereas for CuBr and CuI the opposite is true (the assignment of the observed peaks follows from their intensities; peak Z_1 is larger than peak Z_2 by definition (see also Sec. IV).

The spectrum of CuI (Fig. 3) shows a slight splitting of the exciton $Z_{1,2}$ even for $p=0$, which can be attributed to a differential thermal compression between the sample and the substrate.² At higher pressures this splitting increases, thus proving the existence of a uniaxial component of the applied stress of equal sign to that produced by the differential compression.

If the assumptions made in Sec. II are true for any pressure, one should find a linear dependence of the average position $\bar{Z}_{1,2}$ of the excitons Z_1 and Z_2 on pressure. This energy depends, to first order,

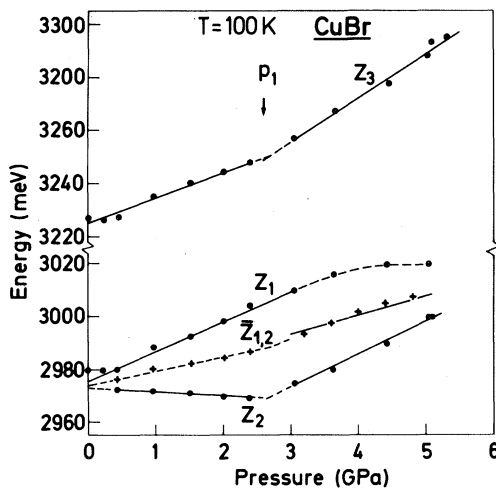


FIG. 5. Shift of Z_1, Z_2, Z_3 and $\bar{Z}_{1,2}$ for CuBr at $T \approx 100$ K. Change in the slopes at $p=2.6$ GPa indicates that the uniaxial component begins to decrease and the pressure becomes more hydrostatic.

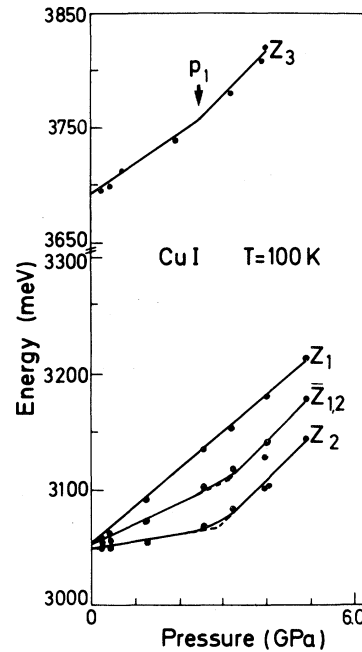


FIG. 6. Shift of the excitons Z_3, Z_2, Z_1 and the average of Z_1, Z_2 labeled as $\bar{Z}_{1,2}$ of a thin film of CuI as a function of pressure p at $T \approx 100$ K.

only on the hydrostatic component of the stress. Moreover, one should find a linear pressure dependence of the splitting between Z_1 and Z_2 , caused by the uniaxial stress component, at least for CuBr and CuI: For these materials linear approximations are good enough within the accuracy of the measurements (see Fig. 12 below). However, Figs. 4–6 show that this is true only for cell pressures p which are smaller than a critical value $p_1 \sim 3$ GPa. For $p > p_1$ the slope of the average position $\bar{Z}_{1,2}$ is larger than for pressures $p < p_1$. Secondly, as shown in Fig. 7 for CuBr, we find a decrease of the splitting between Z_1 and Z_2 with increasing pressure p for $p > p_1$, instead of a linear increase. The same is true for CuCl and CuI.

We infer from these observations that the applied strain becomes more hydrostatic and less uniaxial for pressures above ~ 3 GPa. This is likely to be due to having reached the limit of adhesion to the substrate. The interface with the substrate cannot support the applied shear and the sample pulls loose from it. Consequently, the strain $\epsilon_{xx}, \epsilon_{yy}$ parallel to the substrate is not zero for $p > p_1$ and the assumptions made in Sec. II are no longer true for $p > p_1$. The fluid probably separates the crystallites or penetrates into other cracks and the pressure becomes more hydrostatic than predicted by Eq. (5).

The experiments show that shear-stress com-

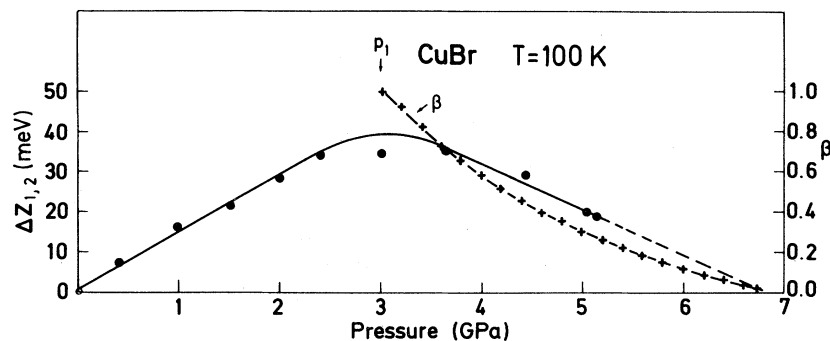


FIG. 7. Pressure dependence of the splitting $\Delta Z_{1,2}$ of the excitons Z_1, Z_2 for CuBr at $T=100$ K. Inversion of the slope indicates that the pressure becomes more hydrostatic. Dashed line with crosses gives the ratio β of the measured splitting to the extrapolation of this linear fit to this splitting found for $p < p_1$, both at the same pressure.

ponents, as described by Eq. (4b), exist at least at low temperatures at which the pressure fluid is glassy. To discuss the influence of the temperature, we compare Figs. 4(a)–4(c) showing the dependence of the energies of the excitons Z_1, Z_2, Z_3 on pressure p for CuCl for three temperatures 100, 200, and 300 K (for the measurements at $T=200$ and 300 K we have used a pentane-isopentane 1:1 mixture as a pressure transmitting medium: The standard methanol-ethanol mixture seems to attack the CuCl samples at least at room temperature). For the other materials the influence of the temperature is in principle the same. In the data at 200 and 300 K we do not see any splitting of the peak $Z_{1,2}$. This can be due to two causes. On the one hand, the excitons broaden as the temperature is increased, thus making the splitting difficult to observe. However, the broadening is not sufficient to account for the lack of splitting. Hence we believe that in this case the uniaxial component of the stress is smaller than for the measurements at 100 K. A comparison of Figs. 4(a) and 4(b) clearly shows that the average shift of the peaks Z_1 and Z_2 for a given $p < 3$ GPa is larger in Fig. 4(b). We thus infer that the hydrostatic pressure p_H , which corresponds to a given cell pressure p , is higher in Fig. 4(b) [see Eqs. (12) and (9)]. The slope of the $Z_{1,2}$ and Z_3 curve in Fig. 4(b) also increases slightly above 3 GPa as uniaxial strain is lifted. At room temperature [Fig. 4(c)] no sign of a uniaxial strain is present. The pressure seems to be purely hydrostatic, as the pressure dependence of the exciton energies is exactly linear in the whole pressure range (below about 5 GPa, where a phase transition takes place). Secondly, the shift of the excitons measured at room temperature agrees with the shift of the absorption edge of bulk crystals under purely hydrostatic pressures. We presume that these temperature effects are related to the decreasing

viscosity of the pressure fluid with increasing temperature.

We have also studied pressure-induced phase transitions of the copper halides. We do not want to give a systematic discussion of them here (see Ref. 7) but wish to show two examples. Figure 4(a) indicates a discontinuous change of the exciton energies at $p=4.8$ GPa for CuCl. We believe it is due to a

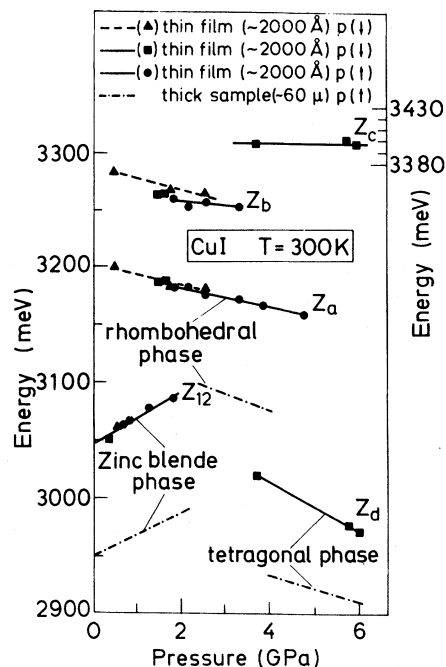


FIG. 8. Pressure dependence of the $\bar{Z}_{1,2}$ (zinc blende), Z_a, Z_b (rhombohedral), and Z_c and Z_d (probably PbO phase) excitons for CuI at $T=300$ K. Dot-dashed lines correspond to the pressure shift of the absorption edge of a thick sample ($\sim 60 \mu$) of CuI. Arrows (\uparrow, \downarrow) indicate an increase (\uparrow) or a decrease (\downarrow) of the pressure p .

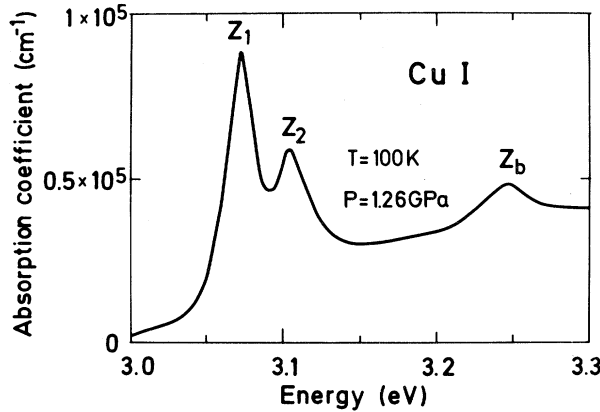


FIG. 9. Absorption coefficient of CuI at $T \approx 100$ K as a function of energy. Inversion of the intensities of the peaks Z_1 and Z_2 is shown. We had warmed up the sample at $T=300$ K and then, after taking some spectra at this temperature at various pressures, we cooled it down again at $T=100$ K to perform these measurements.

phase transition. Another example is given in Fig. 8 where the pressure dependence of the exciton energies at room temperature is plotted for CuI. These curves show phase transitions at $p=2$ and 4 GPa which we could not observe at $T=100$ K (Fig. 6). At 2 GPa a transition, probably to the rhombohedral phase,²⁵ takes place. This transition was hindered at low temperatures, probably because of the uniaxial component of the stress [we note that the c/a ratio of this phase is higher (4.90) than that of the cubic one (4.89)]. A second phase transition, most likely to a tetragonal PbO-like phase,^{8,25} appears at 4 GPa. The rhombohedral phase remains metastable upon decreasing pressure down to $p > 0$. At ~ 6 GPa the rock-salt phase, with an indirect edge, appears. As expected, this phase shows no sharp edge excitons. In Fig. 9 we display the absorption spectrum for CuI at $T=100$ K after having previously warmed up the sample under pressure at room temperature. These data show the peculiarity that the positions of the peaks Z_1 and Z_2 are inverted compared with those in Fig. 3(b). This may be due to a change in the orientation of the crystallites during the warming of the sample. The peak

Z_b in Fig. 9 indicates a small residue of the rhombohedral phase which appears at room temperature under pressure.

IV. DISCUSSION

The main purpose of this section is to discuss how to determine the deformation potentials of the valence bands from our measurements. The uniaxial deformation potentials d_1 and d_2 (Refs. 23, 24, and 26) are of special interest here. d_1 describes the dependence of the top of the valence band on a uniaxial stress along [111] neglecting effects on the spin-orbit interaction. d_2 describes the dependence of the spin-orbit interaction on a [111] strain. Both d_1 and d_2 (expected to be much less than d_1) are small for the copper halides. Therefore high strains, as obtained with our technique, are required for their determination.

The deformation potentials of the top valence bands [a_1, a_2 (hydrostatic) and d_1, d_2 (uniaxial)] are defined as stress coefficients of an expansion of the stress-dependent Hamiltonian in terms of operators which belong to different irreducible representations of the point group of the crystal. (Note that although we talk about band edges, we mean actually the corresponding exciton states. The deformation potentials of the excitons are equal to those of the corresponding band edges, slightly renormalized to account for effects of the strain on the binding energy.) Following the procedure of Ref. 23, the deformation potentials can be formally introduced as parameters of the Hamiltonian for the top valence bands at $k=0$. The total stress-dependent part of the effective Hamiltonian of the upper Γ_{15} valence band can be written as

$$H = H_{so} + H_1 + H_2, \quad (7)$$

where H_{so} is the spin-orbit Hamiltonian in the absence of strain, H_1 is the orbital-strain Hamiltonian, and H_2 is the stress-dependent spin-orbit Hamiltonian. For the [111] strain $\epsilon_{ij} = p/(3C_{11})$ ($i, j = x, y, z$) generated in our experiments, the Hamiltonian matrix of Eq. (7) becomes²³

$$H = \begin{pmatrix} \left| \frac{3}{2}, \frac{3}{2} \right\rangle_{111} & \left| \frac{3}{2}, \frac{1}{2} \right\rangle_{111} & \left| \frac{1}{2}, \frac{1}{2} \right\rangle_{111} \\ -\delta E_H - \frac{1}{2} \delta \omega_0 & 0 & 0 \\ 0 & -\delta E_H + \frac{1}{2} \delta \omega_0 & -2^{-1/2} \delta \omega_0^* \\ 0 & -2^{1/2} \delta \omega_0^* & -\Delta_0 - \delta E_H^* \end{pmatrix}. \quad (8)$$

We have used the equivalent (J, M_J) angular momentum notation for the valence-band wave functions at $k=0$. Δ_0 is the spin-orbit splitting of the Γ_{15} valence band at zero pressure and the following abbreviations have been introduced:

$$\begin{aligned}\delta E_H &= (a_1 + a_2)(\epsilon_{xx} + \epsilon_{yy} + \epsilon_{zz}), \\ \delta E_H^* &= (a_1 - 2a_2)(\epsilon_{xx} + \epsilon_{yy} + \epsilon_{zz}), \\ \delta\omega_0 &= 2\sqrt{3}(d_1 + 2d_2)\epsilon_{xy}, \\ \delta\omega_0^* &= 2\sqrt{3}(d_1 - d_2)\epsilon_{xy}.\end{aligned}\quad (9)$$

a_1 and d_1 are the hydrostatic and the uniaxial deformation potentials of the orbital-strain Hamiltonian H_1 ; a_2 and d_2 are the corresponding coefficients of the strain-dependent spin-orbit Hamiltonian H_2 .

The diagonalization of (8) yields the energies of the three branches of the Γ_{15} valence band as a function of pressure with the deformation potentials as parameters. The energies of the two Γ_8 valence bands are

$$E_1^v = -\delta E_H - \frac{1}{2}\delta\omega_0, \quad (10a)$$

$$E_2^v = \frac{1}{2}(\nu + \xi) + \frac{1}{2}[(\nu - \xi)^2 + 2(\delta\omega_0^*)^2]^{1/2},$$

while the energy of the Γ_7 split-off band is

$$E_3^v = \frac{1}{2}(\nu + \xi) - \frac{1}{2}[(\nu - \xi)^2 + 2(\delta\omega_0^*)^2]^{1/2}, \quad (10b)$$

where

$$\nu = -\delta E_H + \frac{1}{2}\delta\omega_0,$$

$$\xi = -\Delta_0 - \delta E_H^*.$$

To compare the optical-absorption data with the theory developed above, we must also take into account strain effects on the conduction band to calculate transition energies and intensities. The Γ_6 conduction band of the copper halides is affected only by the hydrostatic part of the strain. Introducing a hydrostatic deformation potential c for the conduction band, the strain dependence of the corresponding band energy E_c becomes

$$E^c = c(\epsilon_{xx} + \epsilon_{yy} + \epsilon_{zz}). \quad (11)$$

From (10) and (11) we obtain the energies of the direct interband transitions. These transition energies may be compared with the measured exciton energies if other effects like the influence of strain-induced k -linear terms or the exchange interaction of excitons are not important. The k -linear terms are too small to be observed within the experimental accuracy. However, the effect of exciton exchange does play an important role for CuCl but not for

CuBr and CuI, as we shall see below (see also Refs. 27–29). Hence we may use the Eqs. (10) and (11) to interpret the strain dependence of the exciton energies of CuBr and CuI. However, for CuCl, we have to use a more detailed exciton picture.

We may expand the square root in Eq. (10) in a power series up to first-order terms in δE_H , δE_H^* , $\delta\omega_0$, and $(\delta\omega_0^*)^2/\Delta_0$, since the spin-orbit splitting Δ_0 is large in comparison with the energies defined in Eq. (9). In this way we obtain for the shifts ΔE_1 , ΔE_2 , and ΔE_3 of the direct transitions as a function of a [111] strain $\epsilon_{ij} = p/(3C_{11})$ ($i, j = x, y, z$) defined in (3)

$$\begin{aligned}Z_1: \Delta E_1 &= \delta(E^c - E_1^v) = cp/C_{11} + \delta E_H + \frac{1}{2}\delta\omega_0, \\ Z_2: \Delta E_2 &= \delta(E^c - E_2^v) = cp/C_{11} + \delta E_H - \frac{1}{2}\delta\omega_0 \\ &\quad - \frac{1}{2}(\delta\omega_0^*)^2/\Delta_0, \quad (12) \\ Z_3: \Delta E_3 &= \delta(E^c - E_3^v) = \Delta_0 + cp/C_{11} + \delta E_H^* \\ &\quad + \frac{1}{2}(\delta\omega_0^*)^2/\Delta_0.\end{aligned}$$

In principle one can fit with Eq. (12) the experimental data. The linear terms would yield values for $c + a_1 + a_2$, $c + a_1 - 2a_2$, and $d_1 + 2d_2$; the quadratic terms of (12) would yield $d_1 - d_2$. Thus by fitting with Eq. (12), we could calculate the deformation potentials $c + a_1$, a_2 , d_1 , and d_2 . Unfortunately, the quadratic terms in Eq. (12) are small. Therefore it is not possible in this way to obtain accurate numbers for d_1 , and particularly d_2 , because of the scatter of the few experimental points available.

This problem can be partly overcome by measuring the pressure dependence of the transition intensities. Assuming $\delta E_H, \delta E_H^*, \delta\omega_0, \delta\omega_0^* \ll \Delta_0$ we obtain from the Hamiltonian matrix of Eq. (8) for the intensities $I_{Z_1}, I_{Z_2}, I_{Z_3}$, of the excitons Z_1, Z_2, Z_3 for light propagating along the [111] direction,²⁶

$$\begin{aligned}\frac{I_{Z_1} + I_{Z_2}}{I_{Z_3}} &= \frac{2 - \delta\omega_0^*/\Delta_0 + O((\delta\omega_0^*/\Delta_0)^2)}{1 + \delta\omega_0^*/\Delta_0 + O((\delta\omega_0^*/\Delta_0)^2)} \\ &\simeq 2 - 3(\delta\omega_0^*/\Delta_0).\end{aligned}\quad (13)$$

In Eq. (13) we have neglected second-order terms $O((\delta\omega_0^*/\Delta_0)^2)$: The intensity ratio depends only on $\delta\omega_0^*/\Delta_0$. Thus by measuring the pressure dependence of the relative transition intensities, we can obtain a value for $d_1 - d_2$. This can be more accurate than the value found from a measurement of the exciton energies as a function of pressure.

As mentioned above, Eqs. (12) and (13) hold only for excitons as long as exchange effects are negligi-

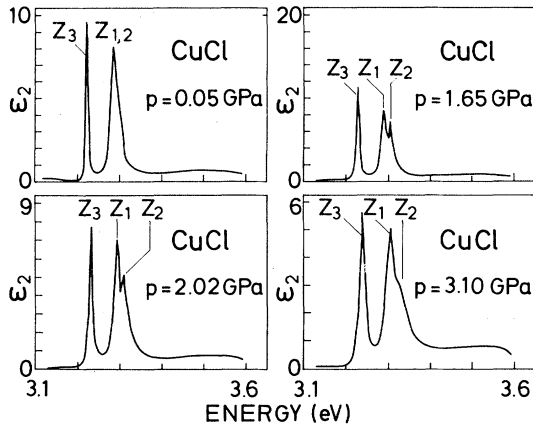


FIG. 10. Imaginary part of the dielectric function of CuCl at various values of the applied pressure at $T=100$ K.

bly small. A way to test this is the measurement of the relative exciton intensities at zero pressure. In the absence of exchange, we obtain from (13) $(I_{Z_1} + I_{Z_2})/I_{Z_3} = 2$. Taking into account the exchange energy λ , the intensity ratio at zero pressure is given by²⁹

$$\frac{I_{Z_1} + I_{Z_2}}{I_{Z_3}} = \frac{1 \pm \left[\frac{(3\lambda - \Delta_0)^2}{8\Delta_0^2 + (3\lambda - \Delta_0)^2} \right]^{1/2}}{1 \mp \left[\frac{(3\lambda - \Delta_0)^2}{8\Delta_0^2 + (3\lambda - \Delta_0)^2} \right]^{1/2}}. \quad (14)$$

The plus sign holds for $\Delta_0/(3\lambda - \Delta_0) < 0$ and the minus sign for $\Delta_0/(3\lambda - \Delta_0) > 0$. In the case of the copper halides the plus sign is appropriate because $|\Delta_0| > \lambda > 0$ (see Table V). If the exchange energy λ is not negligible in comparison with the spin-orbit splitting Δ_0 , there must be a deviation of the intensi-

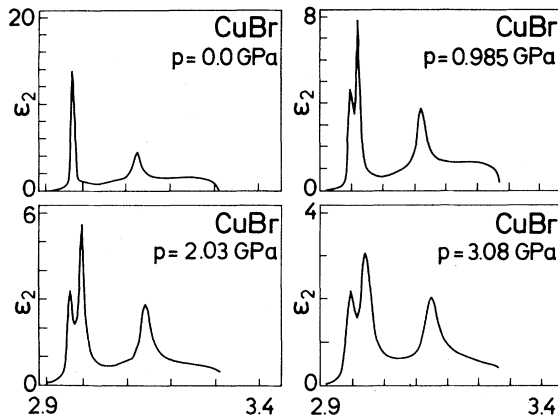


FIG. 11. Imaginary part of the dielectric function of CuBr at various values of the applied pressure at 100 K.

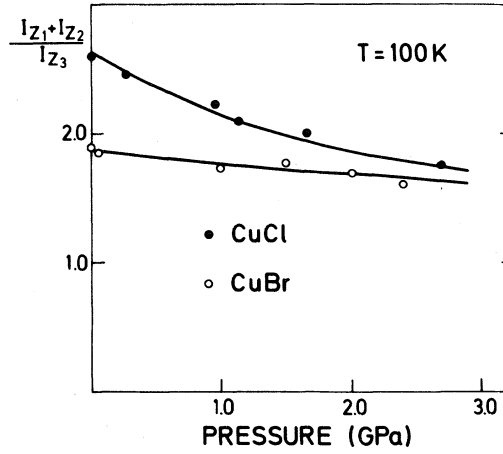


FIG. 12. Pressure dependence of the intensities ratio $(I_{Z_1} + I_{Z_2})/I_{Z_3}$ for CuCl and CuBr at $T=100$ K. Solid curves are fits with eigenvectors of Table III to the experimental data.

ty ratio in Eq. (14) from 2. To first order in λ/Δ_0 this deviation is $-4\lambda/\Delta_0$. Thus, by measuring the intensity ratio of Eq. (14) we obtain a value for λ and we can decide whether exchange effects should be taken into account. We first discuss this point before returning to the evaluation of the deformation potentials.

The relative intensity of the excitons is equal to the ratio of the integrated imaginary parts ϵ_2 of the dielectric function for the experimental peaks. This ratio is not equal to the corresponding ratio of the absorption coefficients, which are not linearly related to ϵ_2 . Therefore we have calculated the ϵ_2 spectra from the absorption spectra in Figs. 1–3 using the Kramers-Kronig relation.³⁰ The results are shown in Figs. 10 and 11 for CuCl and CuBr, respectively.

In order to calculate the intensity ratio of Eq. (14) we have computed the ratio of the peak areas of the ϵ_2 spectra. The relative intensity of Eq. (14) for CuCl and CuBr as a function of pressure p is plotted in Fig. 12. At $p=0$ these ratios are 2.60 ± 0.05 for CuCl and about 1.90 ± 0.05 for CuBr. The corresponding exchange energies λ are 10 ± 2 and 5 ± 2 meV for CuCl and CuBr, respectively. Obviously, the exchange effect is much stronger in the case of CuCl than for CuBr. One can show (see Tables II and III) that the splitting of the $Z_{1,2}$ and the Z_3 exciton at zero pressure is

$$\Delta E = [(\lambda/3 - \Delta_0)^2 + 8\lambda^2/9]^{1/2}. \quad (15)$$

From Eq. (15) we calculate that the deviation of the $Z_{1,2}$ - Z_3 splitting from the spin-orbit splitting Δ_0 of the Γ_8 - Γ_7 band at zero pressure is about 1 meV for

TABLE II. Exchange part of the Hamiltonian (16) with respect to the basis of the exciton states (19a) and (19b). The matrix elements of the triplet states are zero [λ is the so-called electron-hole exchange energy (Ref. 34)].

H_{ex}	$\frac{1}{\sqrt{2}}[x\rangle - y\rangle]$	$\frac{1}{\sqrt{2}}[x\rangle_c - y\rangle_c]$	$\frac{1}{\sqrt{6}}[x\rangle + y\rangle - 2 z\rangle]$	$\frac{1}{\sqrt{6}}[x\rangle_c + y\rangle_c - 2 z\rangle_c]$
	$\frac{2}{3}\lambda$	$\frac{\sqrt{2}}{3}\lambda$	0	0
	$\frac{\sqrt{2}}{3}\lambda$	$\frac{\lambda}{3}$	0	0
	0	0	$\frac{2}{3}\lambda$	$\frac{\sqrt{2}}{3}\lambda$
	0	0	$\frac{\sqrt{2}}{3}\lambda$	$\frac{\lambda}{3}$

CuBr. This is within the experimental accuracy of ± 1 meV. Therefore we assume that exchange effects are negligible for ΔE in the case of CuBr. In the case of CuCl, we find that the $Z_{1,2}$ - Z_3 splitting is about 4 meV smaller than Δ_0 . Thus in order to obtain a good fit to the pressure dependence of exciton energies and the transition intensities for CuCl it is necessary to take exchange effects into account. In the case of CuI it is not easy to obtain good data for the intensity ratio of Eq. (14), because the spin-orbit splitting is very large ($\Delta_0 = 640$ meV) and the sensitivity of the optical instrumentation is not constant over such a large spectral range. Nevertheless, we expect that exchange effects are much smaller than for CuBr, because the exchange energy should be of the same order and the spin-orbit splitting

much larger for CuI than for CuBr.

Following the arguments listed above, we use Eq. (12) to fit the measured pressure dependence of exciton energies of CuBr and CuI and assume that the pressure coefficient of the intensity ratio $(I_{Z_1} + I_{Z_2})/I_{Z_3}$ is $-3\delta\omega_0^*/\Delta_0$ as in Eq. (13). For CuBr we obtain $d_1 - d_2 = 270$ meV. Therefore the quadratic terms in Eq. (12) are small corrections, less than 1 meV for pressures up to 3 GPa: Hence we neglect them. This procedure should be even better for CuI. The deformation potentials we obtain in this way are listed in Table IV. For CuI we have determined $d_1 + 2d_2$ but not $d_1 - d_2$ because of the lack of data for the pressure dependence of the relative exciton intensities.

In the case of CuCl we use a more detailed exci-

TABLE III. Effective Hamiltonian matrix of Eq. (16), using as a basis the exciton states of Eq. (19a) for $K \parallel [111]$ and strain $\parallel [111]$. The Block matrix for the exciton states (19b) is equivalent to that given here. Δ_0 is the spin-orbit splitting of the unstrained crystal.

$ 2, +\rangle$	$\frac{1}{\sqrt{2}}[1, +\rangle - 1, -\rangle]$	$\frac{1}{\sqrt{6}}[x\rangle + y\rangle - 2 z\rangle]$	$\frac{1}{\sqrt{6}}[x\rangle_c + y\rangle_c - 2 z\rangle_c]$
S_1	$i\sqrt{6}X_1$	$-i\sqrt{6}X_1$	$i\sqrt{6}X_2$
$i\sqrt{6}X_1$	$S_1 - \sqrt{3}X_1$	$\sqrt{3}X_1$	$-\sqrt{3}X_2$
$i\sqrt{6}X_1$	$\sqrt{3}X_1$	$S_1 - \sqrt{3}X_1 + \frac{2}{3}\lambda$	$-\sqrt{3}X_2 + \frac{\sqrt{2}}{3}\lambda$
$-i\sqrt{6}X_2$	$-\sqrt{3}X_2$	$-\sqrt{3}X_2 + \frac{\sqrt{2}}{3}\lambda$	$\Delta_0 + S_2 + \frac{\lambda}{3}$

$$\epsilon_{ij} = \frac{1}{3} \frac{p}{C_{\parallel}}, \quad i, j = x, y, z$$

$$S_1 = (a_1 + a_2)(\epsilon_{xx} + \epsilon_{yy} + \epsilon_{zz})$$

$$S_2 = (a_1 - 2a_2)(\epsilon_{xx} + \epsilon_{yy} + \epsilon_{zz})$$

$$X_1 = -\frac{1}{2}(d_1 + 2d_2)\epsilon_{xy}$$

$$X_2 = -\frac{1}{\sqrt{2}}(d_1 - d_2)\epsilon_{xy}$$

ton picture including exchange effects. The effective Hamiltonian formalism described by Cho³¹⁻³³ is used. We diagonalize the Hamiltonian matrix of an effective exciton Hamiltonian of the form

$$H_{\text{eff}} = H^{(c)} + H^{(v)} + H_{\text{ex}}, \quad (16)$$

where $H^{(c)}$ describes stress effects on the conduction band and $H^{(v)}$ takes into account the stress effects on the valence bands, including spin-orbit coupling. H_{ex} is the electron-hole exchange Hamiltonian, which is assumed to be stress independent.

We start with a basis of 12 exciton states of the wave vector $k=0$ consisting of pair states of one hole in one of the Γ_7, Γ_8 valence bands and an electron in the Γ_6 conduction band. Following the notation of Cho,³¹ we can form six singlet states of Γ_5 symmetry and six triplet states of $\Gamma_2, \Gamma_3, \Gamma_4$ symmetry,

$$\begin{aligned} \Gamma_5: & |x\rangle, |y\rangle, |z\rangle, & [2], \\ & |x\rangle_c, |y\rangle_c, |z\rangle_c, & [\sqrt{2}], \\ \Gamma_4: & |1, +\rangle, |1, -\rangle, |2, -\rangle, & [0], \\ \Gamma_3: & |2, +\rangle, |2, 0\rangle, & [0], \\ \Gamma_2: & |0, 0\rangle, & [0]. \end{aligned} \quad (17)$$

The singlet states can be excited by a dipole transition, the triplet states cannot. The numbers in square brackets are the relative magnitudes of the dipole matrix element. x, y, z indicate the polarization of the dipole-allowed states and index c indicates that the exciton is related to a hole in the split-off valence band. For a (J, M_J) angular momentum notation of the wave function of Eq. (17) see Refs. 32 and 33.

The form of the Hamiltonian of Eq. (16) is also given in Refs. 30-32. We need not write the whole matrix and only discuss the results for the eigenstates which can be excited by dipole transitions.

$$\{|2, +\rangle, \frac{1}{\sqrt{2}}[|1, +\rangle - |1, -\rangle], \frac{1}{\sqrt{6}}[|x\rangle + |y\rangle - 2|z\rangle], \frac{1}{\sqrt{6}}[|x\rangle_c + |y\rangle_c - 2|z\rangle_c]\} \quad (19a)$$

and

$$\{|2, 0\rangle, \frac{-1}{\sqrt{6}}[|1, +\rangle + |1, -\rangle - 2|2, -\rangle], \frac{1}{\sqrt{2}}[|x\rangle - |y\rangle], \frac{1}{\sqrt{2}}[|x\rangle_c - |y\rangle_c]\}. \quad (19b)$$

The other exciton functions of Eq. (17), which do not belong to the set of Eqs. (19a) and (19b), correspond to pure triplet states and are of no interest here.

The two sets of exciton states given in Eqs. (19a) and (19b) are independent but equivalent: They yield exactly the same block matrices of the Hamiltonian. Therefore the problem of finding all exciton

Corresponding to the experimental situation, we deal only with the special case $\vec{K}||[111]$ for the incident light and strain parallel to $[111]$ [Eqs. (3) and (4)].

At zero pressure one can observe only transverse singlet states in an optical-absorption experiment (dipole allowed). Therefore it is convenient to perform a transformation of the exciton basis of Eq. (17) which changes the polarized singlet states $|x\rangle, |y\rangle, |z\rangle, |x\rangle_c, |y\rangle_c$, and $|z\rangle_c$ into two sets of transverse states, and one set of longitudinal states with zero oscillator strength. We choose as transverse states

$$\frac{1}{\sqrt{6}}[|x\rangle + |y\rangle - 2|z\rangle], \quad (18a)$$

$$\frac{1}{\sqrt{6}}[|x\rangle_c + |y\rangle_c - 2|z\rangle_c],$$

and

$$\frac{1}{\sqrt{2}}[|x\rangle - |y\rangle], \quad \frac{1}{\sqrt{2}}[|x\rangle_c - |y\rangle_c] \quad (18b)$$

and as longitudinal states

$$\frac{1}{\sqrt{3}}[|x\rangle + |y\rangle + |z\rangle],$$

$$\frac{1}{\sqrt{3}}[|x\rangle_c + |y\rangle_c + |z\rangle_c].$$

The effect of stress and electron-hole exchange interaction can be described as a mixing of the singlet states with each other by the exchange and an admixture of singlet states to the triplet states induced by the stress. In order to find all eigenstates of Eq. (16) which can be observed in an optical-absorption experiment, we have to find all triplet states [Eq. (17)] which are coupled to the transverse singlet states by the stress. It turns out that we can define two independent sets of exciton functions with nonzero oscillator strengths. These are

eigenstates with nonzero oscillator strength and their transition probabilities is reduced to the diagonalization of a 4×4 matrix. In Table II the matrix of the exchange part of the Hamiltonian is listed as introduced by Onodera and Toyozawa.³⁴ The matrix of the complete exciton Hamiltonian referred to the exciton states of Eqs. (19a) and (19b) is given in Table III. The deformation potentials $c + a_1$,

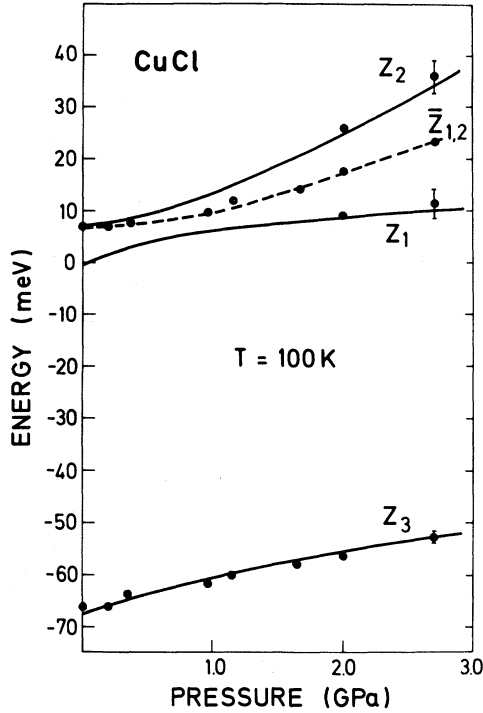


FIG. 13. Energies of the excitons Z_1, Z_2, Z_3 and the average $Z_{1,2}$ of Z_1 and Z_2 as a function of the cell pressure p for CuCl at $T=100$ K. Solid lines are a fit with the eigenvalues of the Hamiltonian in Table III to the experimental data in Figs. 4(a) and 12. Parameters are $\Delta_0 = -70$ meV, $\lambda = 10.2$ meV, and the deformation potentials listed in Table IV.

a_2, d_1, d_2 of Table III have the same meaning as above, i.e., if the exchange is neglected ($\lambda=0$) one obtains exactly the values of Eq. (12) as the eigenvalues of Eq. (20).

For each basis set of Eq. (19) the diagonalization of the Hamiltonian in Table III yields a pure triplet state, which is a mixture of $|2, +\rangle$ and $2^{-1/2}[|1, +\rangle - |1, -\rangle]$ (or, equivalently, a mixture of $|2, 0\rangle$ and $6^{-1/2}[|1, +\rangle + |1, -\rangle - 2|2, -\rangle]$), and three states, which are mixtures of singlet and triplet states. Obviously, these are the three excitons Z_1, Z_2, Z_3 introduced above.

We have fitted the energies calculated for Z_1, Z_2, Z_3 and the intensities of the optical transitions to the experimental data. The results are shown in Figs. 12 and 13. The corresponding deformation potentials are listed in Table IV. In Fig. 14 we display the relative intensities of the optical transitions for Z_1, Z_2, Z_3 calculated with Table III. The theoretical exciton energy curves show a splitting of the excitons Z_1 and Z_2 at zero pressure. This is the singlet-triplet splitting due to the electron-hole exchange ($\lambda=10.2$ meV). At zero pressure Z_1 is a

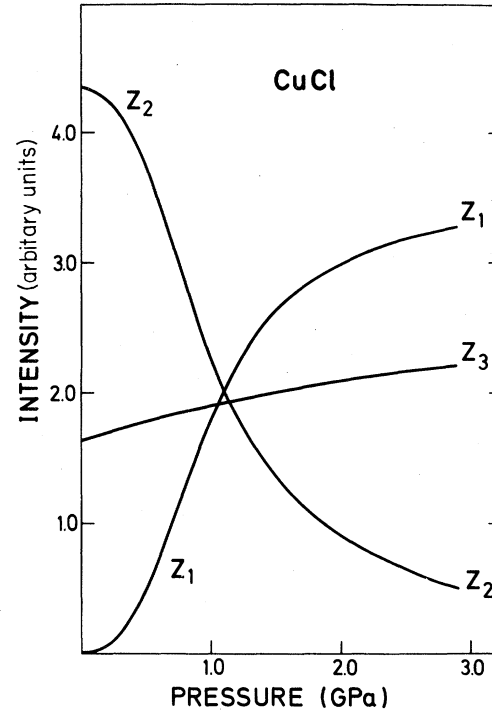


FIG. 14. Intensities of the excitons Z_1, Z_2, Z_3 as a function of pressure p calculated from the Hamiltonian in Table III. Parameters were taken from a fit to the experimental data (Figs. 12 and 13).

pure triplet state with zero oscillator strength. Z_2 is a pure singlet state at zero pressure, i.e., it is either a mixture of the transverse states $2^{-1/2}[|x\rangle - |y\rangle]$ and $2^{-1/2}[|x\rangle_c - |y\rangle_c]$ or a mixture of $6^{-1/2}[|x\rangle + |y\rangle - 2|z\rangle]$ and $6^{-1/2}[|x\rangle_c + |y\rangle_c - 2|z\rangle_c]$. That means that the peak $Z_{1,2}$ in Fig. 1 corresponds to the pure singlet state Z_2 . Nevertheless, this is not in contradiction to the picture we have used above because what we call here Z_2 is a mixture of electron-hole pair states which are related to both branches of the spin-orbit split valence band and coupled by the electron-hole exchange. For pressures $p \neq 0$ the excitons Z_1, Z_2 are not pure triplet or singlet states but an admixture, increasing with pressure, of singlet and triplet states. That is why the transition probability for the Z_1 exciton becomes larger than zero and increases strongly with increasing pressure, whereas the intensity of the Z_2 exciton decreases. For pressures greater than or approximately equal to 1.5 GPa at which a Z_1 - Z_2 splitting is observable in the absorption spectrum (Figs. 1 and 4) the calculation yields that the oscillator strength of the Z_1 exciton is larger than the oscillator strength of the Z_2 exciton (Fig. 14). That proves the assignment of the observed absorption peaks to the calculated exciton states and determines

TABLE V. Electron-hole exchange energies λ (meV) for the cuprous halides determined here and in other publications.

	λ				
CuCl	10 ± 2^a	$9.^b$	19^c	8.7^d	7.4^e
CuBr	5 ± 2^a	2.7 ± 0.6^f	8^c	10^g	2.6 ± 0.6^h
CuI	1.8 ± 0.2^i				

^aThis work. ^dReference 27. ^gReference 1.
^bReference 35. ^eReference 28. ^hReference 36.
^cReference 29. ^fReference 37. ⁱReference 20.

the sign of the deformation potential $d_1 - d_2$, i.e., d_1 since $d_1 \gg d_2$ (see Table IV).

We have also used the matrix of Table III to fit the experimental data for CuBr (Figs. 2 and 12) although the approximations in Eqs. (12) and (13) are sufficient in this case. We checked that fits with the complete matrix of Table III and with Eqs. (12) and (13) yield indeed the same deformation potentials within the experimental errors. We also obtained a value for the exchange energy λ . This should be more accurate than the value we have roughly estimated above. The exchange energies so determined for CuCl and CuBr are presented in Table V and compared with other experimental values.^{1,20,27-29,35-37} Our results for λ are in accordance with the majority of the values determined by other methods. The high values of $\lambda = 19$ meV for CuCl and $\lambda = 8$ meV for CuBr given in Ref. 29 are probably incorrect.

We discuss in what follows the results of Table IV. We have listed in this table for comparison the results of previous measurements of $a_{Z_{1,2}} = c + a_1 + a_2$. In all cases these values are very small when compared with corresponding values of group IV [Ge: $a_{Z_{1,2}} = -13$ eV (Ref. 38)] and group III-V [GaAs: $a_{Z_{1,2}} = -8.6$ eV (Ref. 38)] semiconductors although they have the same sign. There seems to be a systematic decrease of $a_{Z_{1,2}}$ with increasing polarity³⁹: For ZnSe $a_{Z_{1,2}} = -4.1$ eV.³⁹ We note that the $a_{Z_{1,2}}$ measured here for CuBr fits well into the isoelectronic series Ge, GaAs, ZnSe, and CuBr ($-a_{Z_{1,2}} = 13, 8.6, 4.1, \text{ and } 0.3$, respectively). The decrease in $a_{Z_{1,2}}$ with increasing ionicity can be traced to a weak dependence of the ionic component of the gaps (the energy C in Phillip's theory⁴⁰ and V_3 in Harrison's theory⁴¹) on volume. This component seems to be actually nearly independent of volume.⁴² We note that the average deformation potential $a_1 + c$ calculated with the Korringa-Kohn-Rostoker (KKR) (-0.3 eV) and the linear combination of muffin-tin orbitals (LMTO) methods (-1.8 eV)

(Ref. 7) for CuCl also reproduce the experimental trend.

The values of $a_{Z_{1,2}}$ and for $a_{Z_3} = c + a_1 - 2a_2$ measured with different experimental techniques and shown in Table IV are in reasonable agreement with each other except for a systematic trend shown by a_{Z_3} in CuCl. For this material the data obtained with pure hydrostatic stress, without uniaxial component, fall between -0.67 and -1 eV while the data obtained at 100 K for thin films in the presence of hydrostatic stress cluster around -0.4 eV. The difference is well established and two possible explanations arise. One explanation would attribute the difference to a temperature dependence of a_{Z_3} : Most of the data around -0.8 eV were obtained at room temperature while those around -0.4 eV were obtained at ~ 100 K. Nevertheless, the luminescence datum $a_{Z_3} = -0.67$ was also obtained at 100 K. Also, although temperature dependences of a_1, a_2 have been observed,⁴³ the one that would be required to interpret the present data seems to be too large. Also, if one uses in Fig. 4(a) data obtained for $p > 3$ GPa, when the strain is less uniaxial, the deformation potentials a_{Z_3} tend to the "room-temperature" values of 1 eV.

An alternative possibility is that the small coefficient only appears when a large uniaxial stress is present. This would require that the splitting of the cell pressure p into uniaxial and hydrostatic components be shifted from that given in Eqs. (4) and (5) in favor of a larger uniaxial component. It is hard to envisage how this may come about but we recall that CuCl exhibits a number of elastic and thermal anomalies.^{44,45} In any case, more detailed measurements on the same samples at room and low temperatures are necessary to sort out the source of the anomaly reported here.

The deformation potential a_2 is related to the volume derivative of the spin-orbit parameter Δ_0 through $d\Delta_0/d \ln V = -3a_2$. The values of this derivative are listed in Table IV, together with previous determinations published in Ref. 46. Both sets

of data agree within error bars, although the values found on the present work for CuBr seem to be systematically smaller than those of Ref. 7. This marginal discrepancy can be traced to the more elaborate way of extracting the spin-orbit splitting from the data under stress used here, which involves a correction for quadratic terms on strain [Eq. (12)]. This correction lowers the value of $d\Delta_0/d \ln V$ obtained from data under uniaxial strain.

In spite of these quantitative discrepancies it is clear that the spin-orbit splitting increases with increasing hydrostatic pressure. This increase has been interpreted theoretically in Ref. 46 and the discussion will not be repeated here. It suffices to say that in the case of CuCl and CuBr the increase is mainly due to a pressure dependence of the Cu $3d$ -halogen p hybridization of the Γ_{15} valence band. For CuI $d\Delta_0/d \ln V$ is *relatively* (i.e., normalized to Δ_0) smaller than for CuBr and CuCl. In this case $d\Delta_0/d \ln V$ can be explained as arising from the compression of the wave function which results in an increase of their value near the core with increasing pressure.⁴⁶

We note that the values found for d_1 in CuCl and CuBr (or for $d = d_1 + 2d_2$ in CuI) are also rather small. The corresponding values for other zinc-blende-type semiconductors are much larger [-4.7 eV for Ge and -5.3 eV for GaAs (Ref. 38)]. These small values cannot be attributed to the increase in ionicity since $|d|$ for GaAs is actually larger than for Ge. The small values of d must result from the admixture of Cu $3d$ and halogen p wave functions in the Γ_{15} valence bands in a manner similar to that which originates the small values of the deformation potential d_0 for optical phonons⁴⁷ which is related to d through¹⁴

$$d = d' - \frac{1}{4}\zeta d_0. \quad (20)$$

In Eq. (20) d' is the deformation potential in the absence of internal strain while ζ is the internal strain parameter. d' is nearly negligible for Ge.¹⁴ It has not been calculated for the copper halides but if we assume it is also small and neglect it we obtain for CuCl $d \simeq -\frac{1}{4}\zeta d_0 \simeq +0.6$ [$\zeta \simeq 0.9$ for the copper halides⁴⁸ and $d_0 \simeq -2.7$ for CuCl (Ref. 17)]. This argument suffices to explain the sign and the magnitude of d listed in Table IV for CuCl. For CuBr and CuI the magnitude of d_1 (or $d_1 + 2d_2$) is nearly the same but the sign is opposite. We note that according to Ref. 47 d_0 in these materials is still negative and about the same as for CuCl. A small negative value of d' may then account for the observed d .

Concerning the values found for d_2 we can say that they are small, as usual,²⁴ and affected by a large error. Their negative sign is, however, well es-

tablished and beyond the experimental error. We note that this sign is the same as found for Ge (Ref. 24) but opposite to that found for GaAs.²⁴ Since d_2 represents a change of the spin-orbit Hamiltonian produced by the uniaxial strain, it must be related to the strain-induced change in p - d hybridization. It is possible to find a simple relationship between d_2 and a_2 if we assume that the expectation value of the spin-orbit interaction for an orbital \bar{z} directed along the [111] strain axis is only a function of $\epsilon_{\bar{z}\bar{z}}$ i.e., it depends only on the length of the bond along the orbital. Taking $\epsilon_{\bar{y}\bar{y}} = \epsilon_{\bar{x}\bar{x}} = 0$ and $\epsilon_{\bar{z}\bar{z}} \neq 0$ the expectation value of the Hamiltonian H_2 of Eq. (7), given in detail in Ref. 23, for the $L_{\bar{z}} = 1, \sigma_{\bar{z}} = 1$ orbital is

$$a_2 + \sqrt{3}d_2(1 - \frac{1}{3}) = 0, \quad (21)$$

wherefrom we derive (in eV) using the a_2 values of Table IV,

$$d_2 = -\frac{\sqrt{3}}{2}a_2 = \begin{cases} -0.03 & \text{for CuCl} \\ -0.07 & \text{for CuBr} \end{cases}. \quad (22)$$

The values of d_2 predicted in Eq. (22) agree in sign and approximately in magnitude with the measured ones listed in Table IV.

For completeness we have added to Table IV the values of the deformation potential b determined by other authors^{22,49,50} for CuCl and CuBr. This deformation potential represents the splitting of the upper Γ_{15} valence band under a uniaxial strain along [100].

V. CONCLUSIONS

The capability of the diamond anvil cell to perform optical measurements on soft materials (e.g., the copper halides) has been demonstrated. We have studied with this method both the energies and the intensities of the edge excitons of CuCl, CuBr, and CuI under mixed hydrostatic and uniaxial stress. For CuCl the analysis of the data requires the explicit consideration of electron-hole exchange and the diagonalization of a Hamiltonian which includes exchange, spin-orbit interaction, and strain effects. For CuBr the exchange can be treated in perturbation theory. For both of these materials we have obtained from an analysis of the data as a function of strain rather reliable values of the exchange energy. We have also obtained accurate values of the hydrostatic orbital ($c + a_1$) and spin-orbit (a_2) deformation potentials and noticed a discrepancy between the values of ($c + a_1$) for CuCl determined at room and at low temperatures. We have also obtained the deformation potentials for [111] strain labeled d_1 (orbital) and d_2 (spin orbit). The signs and magnitudes of these deformation potentials have been discussed and compared with results for other germanium and zinc-blende-type semiconductors.

ACKNOWLEDGMENTS

We would like to thank Dr. O. K. Andersen, Dr. N. E. Christensen, Dr. D. Glötzel, and Dr. H.

Overhof for help and advice in band-structure-related matters. We also would like to thank Mr. W. Dieterich, Mr. H. Hirt, Mr. M. Siemers, and Mr. P. Wurster for technical help.

*Permanent address: First Laboratory of Physics, Aristotle University of Thessaloniki, Thessaloniki, Greece.

¹A. Goldmann, Phys. Status Solidi B **81**, 9 (1977).

²M. Cardona, Phys. Rev. **129**, 69 (1963).

³A. B. Weinstein and G. J. Piermarini, Phys. Rev. B **12**, 1172 (1975).

⁴B. Welber, M. Cardona, C. K. Kim, and S. Rodriguez, Phys. Rev. B **12**, 5729 (1975).

⁵P. Y. Yu and B. Welber, Solid State Commun. **25**, 209 (1978).

⁶H. Müller, S. Ves, H. D. Hochheimer, and M. Cardona, Phys. Rev. B **22**, 1052 (1980).

⁷S. Ves, D. Glötzel, H. Overhof, and M. Cardona, Phys. Rev. B **24**, 3073 (1981).

⁸O. Brafman and M. Cardona, Phys. Rev. B **15**, 1081 (1977).

⁹G. L. Bir and G. E. Pikus, *Symmetry and Strain-Induced Effects in Semiconductors* (Wiley, New York, 1972).

¹⁰I. Goroff and L. Kleinmann, Phys. Rev. **132**, 1080 (1963).

¹¹E. Kane, Phys. Rev. **178**, 1368 (1969).

¹²U. Gerhardt, Phys. Rev. Lett. **15**, 401 (1965); Phys. Status Solidi **11**, 801 (1965).

¹³P. T. Bailev, Phys. Rev. B **1**, 588 (1970).

¹⁴M. Cardona, *Atomic Structure and Properties of Solids*, edited by E. Burstein (Academic, New York, 1972), p. 514.

¹⁵I. Balslev, in *Semiconductors and Semimetals*, edited by R. K. Willardson and A. C. Beer (Academic, New York, 1972), Vol. 9, p. 403.

¹⁶G. F. Piermarini, S. Block, J. D. Barnett, and R. A. Forman, J. Appl. Phys. **46**, 2774 (1975).

¹⁷S. Hawke, K. Syassen, and W. Holzapfel, Rev. Sci. Instrum. **45**, 1548 (1974).

¹⁸S. Nikitine, L. Wenger-Wusteisen, and J. P. Eberhart, Phys. Kondens. Mater. **2**, 355 (1964).

¹⁹L. D. Bedikyan, V. K. Miloslavskii, and L. A. Ageev, Opt. Spektrosk. **49**, 310 (1980) [Opt. Spectrosc. (USSR) **49**, 167 (1980)].

²⁰L. A. Ageev, V. K. Miloslavskii, and I. T. Maximenko, Fiz. Tverd. Tela (Leningrad) **16**, 2894 (1974) [Sov. Phys.—Solid State **16**, 1873 (1975)].

²¹T. Koda, T. Murahashi, T. Mitani, S. Sakoda, and Y. Onodera, Phys. Rev. B **5**, 705 (1972).

²²S. Sakoda and Y. Onodera, J. Phys. Chem. Solids **32**, 1365 (1971).

²³F. H. Pollak, Suf. Sci. **37**, 863 (1973), and references therein.

²⁴M. C. Chandrasekhar and F. H. Pollak, Phys. Rev. B **15**, 2127 (1977).

²⁵V. Meisalo and M. Kalliomäki, High Temp. High Pres-

ures **5**, 663 (1973).

²⁶F. H. Pollak and M. Cardona, Phys. Rev. **172**, 216 (1968).

²⁷W. Staude, Phys. Status Solidi B **43**, 367 (1971).

²⁸E. Mohler, Phys. Status Solidi B **38**, 81 (1970).

²⁹Y. Kato, C. I. Yu, and T. Goto, J. Phys. Soc. Jpn. **28**, K125 (1971).

³⁰M. Cardona, *Modulation Spectroscopy*, edited by F. Seitz, D. Turnbull, and H. Ehrenreich (Academic, New York, 1969).

³¹*Excitons*, edited by K. Cho (Springer, Berlin, 1979), Chaps. 1 and 2.

³²K. Cho, S. Suga, W. Dreybrodt, and F. Willmann, Phys. Rev. B **11**, 1512 (1975).

³³K. Cho, Phys. Rev. B **14**, 4463 (1976).

³⁴Y. Onodera and Y. Toyozawa, J. Phys. Soc. Jpn. **22**, 833 (1967).

³⁵S. Suga, T. Koda, and T. Mitani, Phys. Status Solidi B **54**, 393 (1972).

³⁶D. P. Vu, Y. Oka, and M. Cardona, Phys. Rev. B **24**, 765 (1981).

³⁷B. Hönerlage, U. Rössler, D. P. Vu, A. Bivas, and J. B. Grun, Phys. Rev. B **22**, 797 (1980).

³⁸*Semiconductors*, Vol. 17a of *Landoldt-Börnstein Tables, New Series*, edited by O. Madelung (Springer, Heidelberg, 1982), Group III.

³⁹D. L. Camphausen, G. A. N. Connell, and W. Paul, Phys. Rev. Lett. **26**, 71 (1971).

⁴⁰J. C. Phillips, *Bands and Bonds in Semiconductors* (Academic, New York, 1973).

⁴¹W. Harrison, *Electronic Structure and Properties of Solids* (Freeman, San Francisco, 1980).

⁴²R. Trommer, H. Müller, M. Cardona, and P. Vogl, Phys. Rev. B **21**, 4869 (1980).

⁴³D. Olego, M. Cardona, and H. Müller, Phys. Rev. B **22**, 894 (1980).

⁴⁴Z. Vardeny and O. Brafman, Phys. Rev. B **21**, 2585 (1980).

⁴⁵S. Levonczuk, J. G. Gross, and J. Ringeisen, J. Phys. (Paris) Lett. **42**, L91 (1981).

⁴⁶A. Blacha, M. Cardona, N. E. Christensen, S. Ves, and H. Overhof, Solid State Commun. **43**, 183 (1982), also in Proceedings of the International Conference on the Physics of Semiconductors, Montpellier, 1982 (in press).

⁴⁷F. Meseguer, J. C. Merle, and M. Cardona, Solid State Commun. **43**, 511 (1982).

⁴⁸R. M. Martin, Phys. Rev. B **1**, 4001 (1970).

⁴⁹T. Koda, T. Mitani, and T. Murahashi, Phys. Rev. Lett. **25**, 1495 (1970).

⁵⁰C. Wecker, A. Daunois, J. L. Deiss, P. Fiorini, and J. C. Merle, Solid State Commun. **31**, 649 (1979).

- ⁵¹R. C. Hanson, J. R. Hallberg, and C. Schwab, Appl. Phys. Lett. 21, 490 (1972).
- ⁵²G. J. Piermarini, F. A. Mauer, S. Block, A. Jayaraman, T. H. Geballe, and G. W. Hull, Solid State Commun.

- 32, 275 (1979).
- ⁵³J. B. Anthony, A. D. Brothers, and D. W. Lynch, Phys. Rev. 5, 3169 (1972).